Biomicrofluidics ARTICLE scitation.org/journal/bmf

A fucosyltransferase inhibition assay using image-analysis and digital microfluidics

Cite as: Biomicrofluidics 13, 034106 (2019); doi: 10.1063/1.5088517
Submitted: 10 January 2019 · Accepted: 29 April 2019 ·
Published Online: 10 May 2019

Laura M. Y. Leclerc,[1,2] Guy Soffer,[2,3] David H. Kwan,[1,2] and Steve C. C. Shih[1,2,3,a)]

AFFILIATIONS

[1]Department of Biology, Concordia University, Montréal, Québec H4B 1R6, Canada
[2]Centre for Applied Synthetic Biology, Concordia University, Montréal, Québec H4B 1R6, Canada
[3]Department of Electrical and Computer Engineering, Concordia University, Montréal, Québec H3G 1M8, Canada

[a)]**Author to whom correspondence should be addressed:** steve.shih@concordia.ca. **Tel.:** +1-(514)-848-2424x7579

ABSTRACT

Sialyl-LewisX and LewisX are cell-surface glycans that influence cell-cell adhesion behaviors. These glycans are assembled by α(1,3)-fucosyltransferase enzymes. Their increased expression plays a role in inflammatory disease, viral and microbial infections, and cancer. Efficient screens for specific glycan modifications such as those catalyzed by fucosyltransferases are tended toward costly materials and large instrumentation. We demonstrate for the first time a fucosylation inhibition assay on a digital microfluidic system with the integration of image-based techniques. Specifically, we report a novel lab-on-a-chip approach to perform a fluorescence-based inhibition assay for the fucosylation of a labeled synthetic disaccharide, 4-methylumbelliferyl β-N-acetyllactosaminide. As a proof-of-concept, guanosine 5′-diphosphate has been used to inhibit *Helicobacter pylori* α(1,3)-fucosyltransferase. An electrode shape (termed "skewed wave") is designed to minimize electrode density and improve droplet movement compared to conventional square-based electrodes. The device is used to generate a 10 000-fold serial dilution of the inhibitor and to perform fucosylation reactions in aqueous droplets surrounded by an oil shell. Using an image-based method of calculating dilutions, referred to as "pixel count," inhibition curves along with IC_{50} values are obtained on-device. We propose the combination of integrating image analysis and digital microfluidics is suitable for automating a wide range of enzymatic assays.

INTRODUCTION

Cell surfaces are densely coated with carbohydrate structures called glycans—assembled through varied linkages from sugar building blocks—which influence signaling mechanisms that control cellular interaction, growth, differentiation, and immune response mechanisms.[1] Changes to the structure and abundance of these glycans are often markers for disease.[2] Fucosylation (addition of a fucose residue) is an important modification to cell-surface glycans. Examples of fucosylated glycans include $Lewis^X$ (Le^X) and sialyl-$Lewis^X$ (sLe^X), whose assembly involves the activity of α(1,3)-fucosyltransferases. Alterations in levels of sLe^X displayed on cell surfaces, resulting from changes in the expression levels of the α(1,3)-fucosyltransferases that assemble them, have been shown to promote higher metastatic potential, drug resistance, and malignancy in a wide range of cancers.[3,4] Toward the discovery of drugs targeting cancer cell-surface glycan modification, the identification of inhibitors for fucosyltransferases addresses metastatic progression and multidrug resistance, having the potential to improve prognoses by preventing malignant disease progression. In addition to their roles in cancer, fucosyltransferases are found to be involved in inflammatory and vascular diseases.[5,6] In certain viral infections, host fucosyltransferases are also transcriptionally activated—for example, by T-cell leukemia retrovirus, herpes simplex virus, cytomegalovirus, and varicella-zoster virus—to increase their infectivity and possibly immune evasion.[7] The bacterium, *Helicobacter pylori,* also takes advantage of fucosylated glycans toward this end, catalyzing their assembly using its own fucosyltransferases. The mimicry of host surface glycans such as Le^X and sLe^X on the cell walls of *H. pylori* is found to play a key role in colonization and adhesion to the host environment.[8] As such, the inhibition of bacterial fucosyltransferases like the α(1,3)-fucosyltransferase of *H. pylori*, FucT, which catalyze the formation of cell-surface glycans such as sLe^X and Le^X, is of clinical importance.

Currently, the search for inhibitors of fucosyltransferases suffers from a lack of high-throughput enzymatic assays that are

efficient, sensitive, and low cost. Compound libraries have previously been screened for inhibitors of specific human fucosyltransferases using TLC- and MALDI-based assays, and microtiter plate-based absorbance- and fluorescence-based assays.[9,10] While these screens have identified some inhibitors, the assay components and the potential inhibitors themselves are often expensive and difficult to obtain in sufficient quantities due to lengthy synthesis and purification processes. Digital microfluidics (DMF) can lower the quantities required to perform these assays, enabling more experiments to be completed at a lower cost.[11]

Generally, microfluidics is described by the manipulation of fluids at micro- to picovolumes for a variety of applications ranging from point-of-care medical diagnostics to the directed evolution of enzymes and microorganisms.[12,13] Among the different microfluidic platforms, DMF allows for the individual addressability of discrete on-chip volumes as droplets—meaning that a number of different operations to move, split, merge, mix, and dispense droplets can be performed on demand. It also benefits from ease of integration with standardized software and affordable electronics that can rapidly generate and respond to feedback based on visual, temperature, and electric signals.[14,15] This ease of integration enables DMF to exhibit an unparalleled potential for analytical detection and responsive automation. For example, DMF is already successful as a miniature and cost-effective platform for enzymatic assays.[11,16] Generally, this application involves dispensing droplets from reservoirs primed with the different assay solutions and then follows with merging and mixing operations such that each droplet is a single bioreactor. Their low volume improves their mass and heat transfer rates, which increases the speed of temperature-variable assays and enzymatic reactions.[17] However, there are challenges in the continued development of DMF technology for screening—such as increasing throughput[18] and reducing the chance of electrode fouling when handling protein-rich solutions.[19,20] Furthermore, in assays that involve many separate steps of component addition, the consistency of dispensed droplet volumes is also pivotal. Specifically for inhibition assays, the ability to obtain inhibition curves that span many orders of magnitude is critical, because these curves can be used to compare the cost and viability of inhibitors.

Here, we report the integration of a high-precision fluorescence-based fucosyltransferase inhibition assay (that we have previously described[10]) on a DMF platform with an image-based analysis tool to screen fucosyltransferase activity and the inhibition of the *H. pylori* enzyme, FucT. We show for the first time an image-based analysis method to calculate droplet volumes and concentrations of an inhibitor, which enabled the generation of dose-response inhibition curves spanning four orders of magnitude for bacterial FucT using GDP (guanosine 5′-diphosphate) as the inhibitor. From this image-based method, we obtain IC_{50} values from the dose–response curves in glycine and nonglycine diluted samples. Next, we also describe a variety of digital microfluidic methodology improvements for implementing enzymatic assays, which include tackling issues in (1) droplet movement and dispensing fidelity and (2) standardization and automation. Specifically, we include a description of a novel electrode design as well as results describing the effects of silicone oil on enzymatic reagents and a description of a standardized imaging tool integrated with our automation system to correlate an image of the droplet to its concentration. Overall, this work is an important first step in our efforts (and others) to standardize automated complex enzymatic analyses on digital microfluidic devices.

MATERIALS AND METHODS

Reagents and materials

Unless specified otherwise, general-use chemicals and kits were purchased from Sigma-Aldrich (St. Louis, MO). Recombinant expression of the enzymes used for this study was carried out following procedures similar to those described previously.[21] Solutions used for the fucosylation assay consisted of an 80 mM GDP solution, a 0.135 mg/mL FucT solution, a reaction-initiating "glycosylation" solution (40 mM $MgCl_2$, 0.04 mM MU-β-LacNAc, and 0.08 mM GDP-fucose), and a reaction-stopping "hydrolysis" solution (125 mM EDTA, 0.25 mM BgaA, and 0.25 mM SpHex). All solutions were prepared with either a 50 mM pH 7.5 Tris or a 25 mM pH 7.0 HEPES buffer. With the volumes of the GDP solution, FucT solution, "glycoslyation" solution, and "hydrolysis" solution combined in the ratio 2:1:1:1, the highest concentration of GDP at the time of the reaction was ∼40 mM. Concentrations in the "glycosylation" mix were 10 mM $MgCl_2$, 0.01 mM MU-β-LacNAc, and 0.02 mM GDP-fucose and concentrations of "hydrolysis" components at the hydrolysis step were of 25 mM EDTA, 0.05 mM BgaA, and 0.05 mM SpHex. All solutions described contained 0.05% Pluronics F-68.

Microfluidic device fabrication reagents and supplies included chromium-coated glass slides with S1811 photoresist from Telic (Valencia, CA), indium tin oxide (ITO)-coated glass slides, $R_S = 15–25\ \Omega$ (cat. no. CG-61IN-S207, Delta Technologies, Loveland, CO), FluoroPel PFC1601V from Cytonix LLC (Beltsville, MD), MF-321 positive photoresist developer from Rohm and Haas (Marlborough, MA), CR-4 chromium etchant from OM Group (Cleveland, OH), AZ-300 T photoresist stripper from AZ Electronic Materials (Somerville, NJ), and DuPont AF from DuPont Fluoroproducts (Wilmington, DE). Transparency masks for device fabrication were printed from CAD/Art (Bandon, OR) and polylactic acid (PLA) material for 3D printing were purchased from 3Dshop (Mississauga, ON, Canada). Deionized (DI) water had a resistivity of 18 MΩ cm at 25 °C. The permanent double-sided tape was purchased from Amazon Canada (3M Scotch).

Automation setup and device operation

The automation system (see Fig. S1 in the supplementary material for hardware connectivity) consisted of Python 2.7 in-house made software used to control an Arduino Uno microcontroller (Adafruit, New York, USA). Driving input potentials of 120–160 V_{RMS} were generated by amplification of a square wave output from a function generator (Agilent Technologies, Santa Clara, CA) operating at 15 kHz by a PZD-700A amplifier, (Trek Inc., Lockport, NY) and delivered to the PCB control board.[11,22] The Arduino controlled the state of high-voltage relays (AQW216 Panasonic, Digikey, Winnipeg, MB) that were soldered onto the PCB control board. The logic state of an individual solid-state switch was controlled through an I^2C communication protocol by an I/O

expander (Maxim 7300, Digikey, Winnipeg, MB). This control board was mated to a pogo pin interface (104 pins), where each switch delivered a high-voltage potential (or ground) signal to a contact pad on the DMF device. See our GitHub registry (https://github.com/shihmicrolab/Automation) to assemble the hardware and to install the open-source software program to execute the automation system.

As shown in Fig. 1(a), the device layout designed in AutoCAD featured an array of 93 actuation electrodes (average width ~1 mm) connected to 10 reservoir electrodes (2 variants, $4.1 \times 3\ \text{mm}^2$ ea.), with an average of interelectrode gap size of 30 μm. Each electrode was connected to a square contact pad at the edge of the chip using 70 μm wide lines. When the devices were mounted, each contact pad was in contact with a pin connected to the electrical setup. When applying an electric field to an electrode, the dielectric layer was polarized such that it enabled droplets to move to an adjacent electrode via electrostatic force. Droplets were grounded via contact with an indium tin oxide (ITO)-coated glass plate which was joined

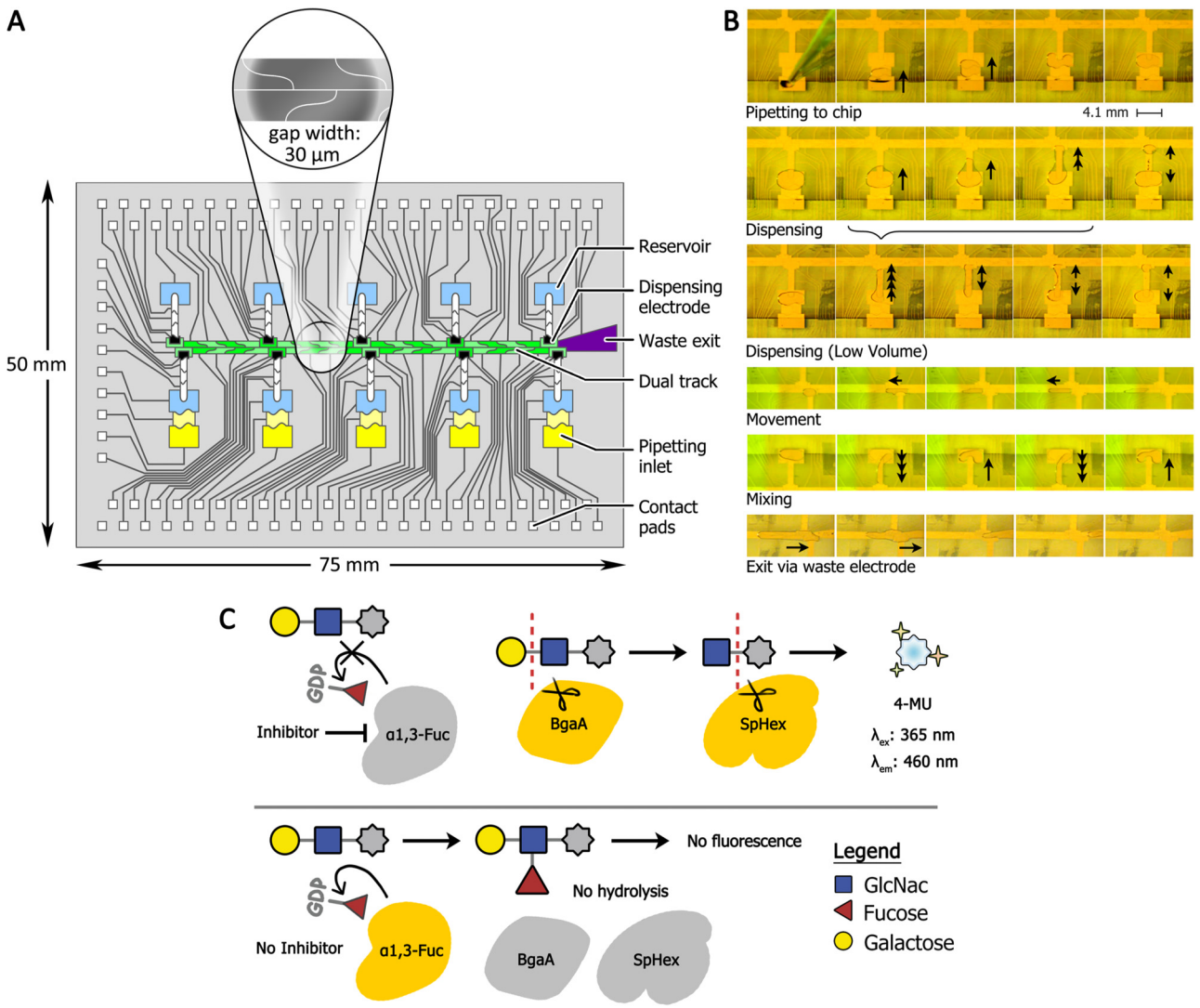

FIG. 1. DMF design for a MU-β-LacNAc-based glycosylation assay. (a) $3 \times 2\ \text{in.}^2$ digital microfluidics chip design comprising 103 electrodes among which are a waste collection electrode, two adjacent tracks connecting every section, and 10 reservoirs. Five reservoirs include pipetting inlets, with a zoomed-in view of a skewed-wave electrode used on the track. (b) Step-by-step depiction of the different operations performed on-device. (c) Schematic of a fucosylation assay. Top: Glycoside hydrolases β-gal from *S. pneumoniae* (BgaA) and *N*-acetylhexosaminidase from *S. plicatus* (SpHex) sequentially cleave synthetically methylumbelliferated disaccharide, MU-β-LacNAc, into its monosaccharide components, releasing fluorescent 4-methylumbelliferone (4-MU). Bottom: Fucosylation by an α(1,3)-fucosyltransferase prevents hydrolysis by BgaA and SpHex; with the 4-methylumbelliferyl oligosaccharide intact, fluorescence remains low.

to the chromium electrode-bearing bottom plate by two layers of double-sided tape to a gap height of approximately 140 μm. Aqueous solutions were either pipetted directly onto the reservoirs before the ITO was added or pipetted to one of five exposed pipetting inlet electrodes that have been aligned to the edge of the ITO. These electrodes, for which a third of the surface area was positioned under the ITO, could pull droplets underneath the ITO whenever actuated. Droplet operations [Fig. 1(b)] were visualized by a 3.0 MP CMOS Color USB camera (EO-3112C, Edmund Optics, New Jersey, USA) attached to a 10× C-mount close focus zoom lens (54363, Edmund Optics, New Jersey, USA). Generally, all droplets containing proteins were supplemented with 0.05% Pluronics F-68. Waste and unused fluids were removed by delivering them to reservoirs and removed using paper strips at the waste reservoir (similar to the study in Ref. 23).

Automation software

We designed a program called "PaseMaker" (i.e., Path Sequence Maker) to construct electrode sequences for any DMF chip design (see the supplementary material for detailed description with figures). Briefly, users provided a .csv file referencing each electrode on a DMF device by its pin number (a sample .csv file is uploaded on GitHub). The first column (or the first number of each line) on this file consisted of the pin number for an electrode, and subsequent columns (or numbers separated by commas on the same line) were pin numbers for the electrodes connected to the reference. The user loaded this file (showing the connectivity) with PaseMaker, which constructs a nonvisual graph to map out the DMF chips as nodal networks describing every connection between electrodes. To generate sequences, the user provided a pin number for two electrodes at opposite extremities of the desired operation (e.g., dispense, move, mix, etc.), and then they clicked the button named after the desired operation. PaseMaker solved the shortest path between those extremities and constructed a string representing the electrode actuation sequence for that operation. When creating this electrode actuation sequence, the user had the option to structure an output string in which up to six output variables can be defined in addition to the electrode actuation sequence. In our case, we organized the output string to include parameters required by the automation system such as seqCategory (a user-defined group of sequences), seqName (a user-defined label for the sequence), seqDesc (a more detailed description describing the droplet sequence), seqList (in which electrodes are turned on in the sequence; this was the variable to which PaseMaker would append the generated electrode sequence), seqOnTime (the time for an electrode to be "on"), and seqPeriod (the time between actuations). Next, a set of python commands was rapidly created and these commands were saved in a user-generated protocol python file, which provided the instructions for the automation system. A GUI was created (called LLGUI.exe) to be used as an interface for the program (Fig. S2 in the supplementary material). Here, the user loaded the protocol file to LLGUI, which automatically creates buttons for each saved droplet operation sequence. Here, these sequence buttons were grouped under their similar droplet operation categories (dispensing, movement, mixing, and storing in reservoirs) to facilitate organization and visual interpretation. An additional text input box (named "#actuations") allowed the user to specify the number of repeats desired for the sequence. Hovering over a button displayed the tooltip (i.e., the sequence description) and clicking the button copied the command string to the clipboard which can be pasted in the python shell to start the sequence actuation (Fig. S3 in the supplementary material). We also included in this software "ArduBridge," which was the Python framework for the Arduino to interpret instructions from the protocol file and to switch the target pin(s) to a desired output state (high voltage or ground) for a specified time according to the electrode actuation sequences. This framework also used the pySerial.py open-source module (see http://pypi.python.org/pypi/pyserial) to access the USB port and communicate with the Arduino.

To detect the droplet area, we followed a protocol similar to that of Vo *et al.*[15] Briefly, the algorithm initially acquired an image that shows the droplet to be measured and was binarized (i.e., digitizing the image to 1's and 0's) to intensify the droplet boundaries. Next, we manually used a "cut-out" algorithm (similar to a lasso tool) to trace the droplet boundary to measure the diameter of the droplet. The droplet volume was calculated using a 140 μm gap height between the two plates multiplied by the area of the droplet.

Optimization and testing of the fucosylation assay

Optimal FucT concentration and hydrolysis reaction times were determined using the ClarioSTAR® well-plate reader. With a negative control (0 nM FucT), seven concentrations of FucT were tested, spanning from 0.09 nM to 1.29 nM. Start and stop solutions, each containing 770 μl, were prepared and primed into separate injectors. 11 μl of negative control and every FucT concentration were added to each well in advance. To start the experiment, the reader automatically injected 9 μl of glycolysis solution in each well. After 10 min, 20 μl of hydrolysis solution were machine injected, followed by a 4-methylumbelliferyl (4-MU) fluorescence reading every minute for 10 min. A ClarioSTAR® monochromator microplate reader (BMG Labtech, Ortenburg, Germany) was used to measure fluorescence from 4-methylumbelliferone (4-MU) using 40 flashes at $\lambda_{ex} = 360$ nm and $\lambda_{em} = 450$ nm at 25 °C. Gain and focal height were optimized by the ClarioSTAR® software before each experiment using a 25 μl 4-MU, 50 mM Tris solution. Well-plate assays were conducted in Nunc™ 384-well polystyrene black microplates (Thermo Scientific™). Each of these experiments was repeated in triplicate. All of the measurements were blank corrected with a solution without any 4-MU.

To generate inhibition curves in a well plate, a blank (0 mM GDP) and six GDP solutions were manually prepared in fourfold dilutions to obtain a range from 0.04 mM to 40 mM. We followed a 4-step protocol to measure the inhibition of FucT by GDP through fluorescence measurements. In step 1, 5 μl of FucT solution were added to 10 μl of GDP solution and incubated for 5 min at room temperature. In step 2, 5 μl of glycosylation mix were added to the above mixture followed by 10 min of incubation at room temperature. In step 3, 5 μl of hydrolysis mix were added to the above mixture followed by 5 min of incubation at room temperature. In step 4, we used the ClarioSTAR® with settings as previously described to measure the fluorescence. Each of these experiments was repeated in triplicate. All of the measurements were blank

corrected using a blank 50 mM Tris solution. A pipette tip covered with silicone oil was immersed into the solution such that the solution in the well was covered with a thin layer of silicone oil and each solution was supplemented with 0.05% Pluronics F-68.

GDP IC_{50} inhibition curves on the device were collected using a 42-step protocol for the DMF device (Fig. S4 in the supplementary material). In step 1, five droplets (~2.7 μl each) of 25 mM HEPES buffer were manually pipetted onto the reservoirs after which the ITO plate was placed on top of the device. In step 2, a 3.1 μl droplet of the inhibitor (i.e., 80 mM GDP) was added to the edge of the ITO (aligned with a reservoir electrode) and the droplet was loaded into the reservoir by applying a driving potential on the reservoir. All solutions were covered with a thin layer of silicone oil by coating a pipette tip with silicone oil and touching the surface of the droplet with the coated tip. In step 3, a unit droplet of GDP (~500 nl) was dispensed from the reservoir. In step 4, the dispensed droplet was added to a reservoir primed with buffer and mixed by pulling the liquid out of the reservoir along the linear path and then actuating the reservoir electrode to pull the entire volume back into the reservoir. This created a dilution of ~1:5. In step 5, a unit droplet of the dilution was dispensed. In steps 6–10, steps 4–5 were repeated with subsequent reservoirs containing only buffer to generate six different inhibitor concentrations (36.0 ± 4.25, 6.2 ± 0.4, 1.1 ± 0.01, 0.22 ± 0.01, 0.04 ± 0.006, and 0.006 ± 0.001 mM), which were calculated using our image-based method. In step 11, a 3.1 μl droplet containing the negative control (a 25 mM HEPES buffer without an inhibitor) was added to an empty reservoir (as in step 2). In step 12, two-unit droplets (500 nl each) were dispensed from the first of the seven GDP concentrations, each occupying a separate reservoir. The unit droplets were merged into a two-unit droplet (1 μl) and actuated away from the path leading to the reservoir. In step 13, the excess droplet in the reservoir was actuated to the waste electrode and wicked away using a paper strip. The two-unit droplet was then returned to its reservoir. In steps 14–19, steps 12 and 13 were repeated for the other six concentrations of GDP (incl. 0 mM). In step 20, a 3.1 μl droplet of FucT was added to the reservoir (as in step 2) and a unit droplet (~500 nl) was dispensed and mixed with the 1 μl GDP droplet in its reservoir. In steps 21–26, step 20 was repeated for the other six concentrations of GDP. In steps 27–33, after 5 min of incubation, seven ~500 nl glycolysis solution droplets were dispensed and added to each reservoir containing a droplet of FucT and GDP. In steps 34–41, after 10 min of incubation, seven ~500 nl droplets of hydrolysis solution were added to each reservoir containing a droplet of FucT, GDP, and glycolysis solution. In step 42, digital microfluidic devices were aligned and mounted to a Nunc™ 384-well-plate, in which fluorescence was scanned at a focal height = 15.80 mm, gain = 750, and with 40 flashes. Custom plate and well dimensions were input to produce fluorescence heatmaps of the entire selected chip surface in 30 × 30 pixel increments, wherein each pixel represented 10 mm^2 of the surface of the device.

RESULTS AND DISCUSSION

Application of a fucosylation assay to test FucT activity and inhibition

To screen for potential inhibitors of the fucosyltransferases involved in the assembly of $Lewis^X$ and sialyl-$Lewis^X$, we previously developed a fluorescence-based inhibition assay to detect the fucosylation of the labeled synthetic disaccharide, 4-methylumbelliferyl β-N-acetyllactosaminide (MU-β-LacNAc).[10] MU-β-LacNAc itself was not strongly fluorescent, but upon hydrolysis by specific enzymes, a brightly fluorescent 4-methylumbelliferone (4-MU) is released [Fig. 1(c)]. The β-galactosidase from *S. pneumoniae* (BgaA)[24] and *N*-acetylhexosaminidase from *S. plicatus* (SpHex)[25] can sequentially act upon MU-β-LacNAc, hydrolytically cleaving galactose and *N*-acetylglucosamine residues, respectively, to release 4-MU. However, fucosylation of the labeled oligosaccharide prior to this treatment results in a structure that was not recognized by the glycosidases, preventing hydrolysis and the subsequent fluorescent signal.[10] With this setup, we tested the activity and inhibition of the *H. pylori* α(1,3)-fucosyltransferase, FucT, which uses GDP-fucose as the nucleotide sugar donor.[26] We first tested this assay using FucT in microtiter plates as a point of comparison to our DMF platform.

We confirmed that our preparation of SpHex and BgaA could indeed hydrolyze MU-β-LacNAc in the absence of fucosylation catalyzed by FucT. In a well plate, a solution with 10 μM MU-β-LacNAc, 10 mM $MgCl_2$, and 50 mM Tris was incubated for 10 min with the presence or absence of BgaA and SpHex at 0.05 mg/ml concentrations. As shown in Figs. 2(a) and 2(b), it was observed that SpHex and BgaA must both be included in the reaction to release a signal equivalent to ~6 μM 4-MU from 10 μM MU-β-LacNAc (***$p < 0.01$). To determine the optimal concentration and time required for inhibition, a range of FucT concentrations from 0 to 0.07 mg/ml were incubated for 10 min with the initial glycosylation solution (10 μM MU-β-LacNAc, 0.02 mM GDP-fucose, 10 mM $MgCl_2$, and 50 mM Tris). After the addition of the initial hydrolysis solution (0.05 mg/ml BgaA, 0.05 mg/ml SpHex, 500 mM EDTA, and 50 mM Tris), fluorescence was measured each minute for 10 min. It was observed that fluorescence for each of the FucT concentrations reached a plateau within 5 min [Fig. 2(c)]. Given these results, 5 min was selected as the optimum length of time required for the hydrolysis step. A FucT concentration of 0.03 mg/ml (0.6 nM) was chosen, given that the maximum fluorescent signal observed at that concentration was sufficiently lower (~20% of the maximum signal, corresponding to ~10 μM 4-MU as reported by the 4-MU standard) compared to the lower concentrations of FucT (<0.01 mg/ml). Although a baseline fluorescence was observed up to around the signal of ~1 μM 4-MU, this selection provides a wide effective range of fluorescence for the assay to distinguish between the strength of inhibitors. Additionally, we observed a minimal baseline fluorescence which we attribute to the slight fluorescence of 4-methylumbelliferyl glycosides vs 4-MU. Finally, we compared the precision of this test by repeating the prior experiment with a single reading after 5 min and for two FucT concentrations—0.6 nM as a negative control (no hydrolysis solution; minimum fluorescent signal) and 0 nM as a positive control (with hydrolysis; maximum fluorescent signal). Overall, this assay yielded Z-factor = 0.78 (n = 8), which was comparable to other fucosyltransferase assays[10] and, therefore, showed promising results for future high-throughput applications.

Next, we tested the inhibition of FucT. Previously, the nucleoside diphosphate GDP had been shown to be a weak (IC_{50} = 0.05 mM)

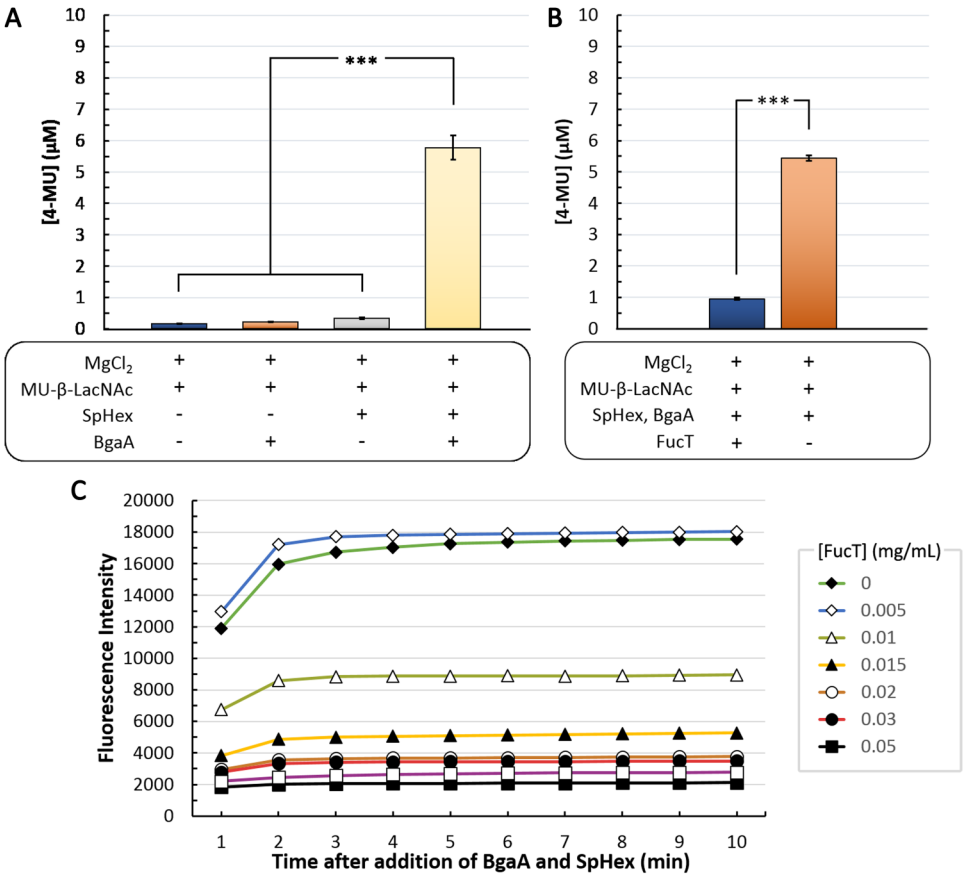

FIG. 2. Design of an inhibition assay. Experiments conducted in a well plate. (a) Graph showing the effect of having a MU-β-LacNAc, SpHex, and BgaA. The 4-MU product produced a fluorescent signal only if cleaved by both glycoside hydrolases (n = 3). (b) Graph showing the effect of FucT. Assay performed with and without 0.6 nM FucT (n = 8). (c) Plot showing fluorescence intensity (y-axis) plotted against time (x-axis) for different FucT concentrations (legend—right side). When MU-β-LacNAc was incubated in 50 mM Tris (pH 7.5) with $MgCl_2$, GDP-Fuc and different concentrations of FucT, the resulting fluorescent signal was inversely related to the concentration of FucT. Fluorescence was measured once per minute for 10 min, showing that the time to completion of the hydrolysis is around 5 min. All graphs with error bars represent one standard deviation. ***p < 0.01.

inhibitor for a recombinant human α(1,3)-fucosyltransferase via monitoring the fucosylation of di- and trisaccharides into tri- or tetrasaccharides.[27] As such, GDP was used as a proof-of-concept inhibitor for the fucosylation of MU-β-LacNAc by *H. pylori* FucT. A blank and ten GDP concentrations ranging from 0.08 mM to 40 mM during the reaction step were incubated with 0.6 nM FucT. This yielded half of the maximal GDP inhibition at $IC_{50} = 0.25 \pm 0.10$ mM (Fig. S6 in the supplementary material). These results were in accordance with GDP's weak profile as an inhibitor as well as the assay's model, in which the fucosylation of MU-β-LacNAc prevents its hydrolysis, and consequently, the fluorescent signal produced by the release of 4-MU is observed only when FucT has been inhibited.

Optimization of fucosylation inhibition assay for digital microfluidics

There have been previous reports that describe the use of digital microfluidics for enzymatic reactions in droplets filled with either oil[28] or air[11] as a filler medium. Here, we introduced the integration of a fucosyltransferase enzyme inhibition assay on DMF using an oil shell and air medium configuration. To our knowledge, the oil shell with the air medium setup was described only in two different works,[29,30] and although both of these systems were characterized, no biological application was presented or the range of tested concentrations was minimal (only one order of magnitude). Here, we described the first fucosylation inhibition assay performed on DMF using this configuration. We also generated proof-of-principle results testing concentrations over multiple orders of magnitude, followed by a comparison to gold-standard techniques (e.g., well-plate techniques). A chip was designed, which brought several novel features to the area of digital microfluidic designs for enzymatic assays, allowing a variety of droplet operations on the device using our automation system. In the work reported here, we used a two-plate configuration (as opposed to a one-plate one) to minimize droplet evaporation and permit droplet dispensing.

In initial experiments, droplet dispensing failure was experienced with assay reagents containing proteins such as FucT, BgaA, or SpHex. We hypothesized that this is most likely due to protein biofouling (i.e., where proteins adhere to the hydrophobic surface of the device). To minimize droplet dispensing failures, five reservoirs were connected to additional pipetting inlet electrodes such that the solutions would rest on the reservoir for a minimal length of time. The ITO top plate was aligned with a third of the inlet electrode's surface, and by applying a driving potential to this inlet, the solution was loaded into the gap between the ITO and the

DMF surface [see Fig. 1(b) "pipetting to chip" and Fig. S4 in the supplementary material for loading steps]. These droplets could then be used immediately for the assay without having it previously rest on the chip, where it could slowly "foul" the surface and dispense droplets from reservoirs with minimal variability (~9%, see Fig. S5 in the supplementary material; also see Ref. 31 for alternative solutions to dispense with minimal variability).

In addition to droplet dispensing failures, we also experienced droplet movement failures with these protein-rich solutions. Two factors affecting droplet movement on DMF were studied: (1) the composition of reagents from the properties of their solutes to the overall pH[32–34] and (2) the shape and size of electrodes relative to droplet volumes.[35] Many labs have addressed the former via the addition of tri-block copolymers of poly(ethylene oxide) (PEO) – poly(propylene oxide) (PPO) – PEO or "Pluronics" (BASF, Florham Park, NJ) to their solutions, some of which have been shown to increase the fouling threshold of protein concentrations for DMF by 1000-fold and to permit over 100 steps of droplet movement to be performed on otherwise biofouling reagents.[32,33] An alternate solution is to surround the droplets in an oil shell or medium to minimize the fouling and evaporation of droplets. Hence, we conducted an experiment to determine the conditions in which the protein solutions used in the fucosylation assay would become capable of movement on the DMF device. The movement of droplets containing each of the proteins was separately tested to discern which of them held the strongest biofouling capacity, and it was determined from our initial experiments that BgaA was the least capable of droplet movement. Speculatively, this could be due to its large size (~247 kDa, which is 4.5 times the mass of SpHex and FucT) since larger molecules do not flow past each other as easily and are more polarizable—in which both of these factors could increase the viscosity of the liquid. As such, 0.05 mg/ml BgaA solutions were prepared with three different surfactant conditions: no surfactant and 0.05% Pluronics F-68 with and without an oil shell. We also speculated that buffer conditions have an effect on droplet movement, and hence, we prepared solutions with three different buffer conditions: no buffer, 50 mM Tris, and 25 mM HEPES for a total of nine test solutions. Using the automation system, we manipulated the droplet between two terminal electrodes in a span of four electrodes to implement the worst-case scenario until either movement failed three times consecutively or movement was successful 24 times (three times more than the maximum number of movements expected across any electrode for this work). As shown in Fig. 3(a), without the addition of surfactant, solutions were immobilized from the start. When 0.05% Pluronics F-68 was added to each of the three buffer conditions, droplet movement improved. Interestingly, without silicone oil, buffer composition also has an impact on droplet movement, in which fouling occurred after (on average) four movements for 50 mM Tris-HCl and after eight movements for 25 mM HEPES buffer. We are unsure of the cause, but we speculated that higher ionic strength prevents the "salting-in" biofouling of molecules or the pH of buffers, which could cause the degradation of the hydrophobic layer.[34] The most notable improvement of droplet movement came with the application of both 0.05% Pluronics F-68 and the addition of an oil shell to BgaA solutions prepared with either buffer. Although movement stopped at 24 actuations, the droplets did not show any signs of slowing down. As a result of these tests, 0.05% F-68 with an oil shell and HEPES buffer were used to perform all subsequent runs of the fucosyltransferase inhibition assay.

With the composition of assay solutions optimized for movement, the second aforementioned factor concerning droplet mobility was examined. Droplet movement on a DMF device depended on the electric field between the top and the bottom plates and was affected by the shape of the electrodes. Electrodes typically are of the shape of a square or a rectangle, and what is noteworthy is the simplicity of drawing these shapes and the ease of their fabrication; however, droplets are known to become stranded (or "static") on an electrode when these volumes fail to overlap with adjacent electrodes ceasing all movement.[36] In response, our group and others have designed interdigitated (e.g., "comb" or "zig-zagged" edges) or otherwise original electrode shapes (e.g., crescent).[12,37] Although this allows droplet movement for smaller volumes than simple rectangular electrodes, pointed shapes created regions with high electric fields $>10^8$ V/cm which can cause dielectric breakdown.[38] To alleviate this problem, intercalating electrodes were created with sinusoidal curves and minimum angles of ~90° where its edges join together, referred to as "skewed-wave" shaped (Fig. S7 in the supplementary material). Their dimensions ($\sim 4.0 \times 0.87$ mm^2) were chosen such that droplets were moved across the intercalating electrodes in both lateral directions. The choice of the sinusoidal curve allowed a droplet to overlap with the adjacent electrode to ensure droplet movement onto the adjacent (i.e., activated) electrode. The length of these electrodes presented a second advantage: droplets were bridged through long distances across the chip with fewer number of electrodes and actuations. If square electrodes of the same area (1.87×1.87 mm^2) were used for the linear track, it would require up to nine electrodes to bridge the length of four skewed waves, reducing the number of electrodes by more than half. However, to avoid droplets becoming static, the minimum volume that could be moved on these square electrodes would be ~27% higher than on skewed-wave electrodes. Square electrodes of the same height could be used to span the distance of four skewed-wave electrodes without increasing the area or minimizing volumes, but in this case, 13 electrodes would be required. This is the first time that such an electrode shape is presented, and it can be used for experiments requiring reliable droplet movement with limited space on the substrate or limited pins/switches in the automation system.

One of the major concerns in using an oil shell is the possible interactions it has with the constituents inside the aqueous droplet. Hence, we tested the impact of silicone oil on 4-MU fluorescence by preparing two standards (with and without silicone oil) at 0.05% Pluronics F-68 concentration. As shown in Fig. 3(b), silicone oil in Pluronics F-68 was not found to impact the fluorescence of a 4-MU standard (N.S.: $p = 0.143 > 0.05$). We also tested another surfactant called ethylenediamine tetrakis(ethoxylate-block-propoxylate) tetrol (Tetronics 150R1), which contains a tetra-functional block copolymer as opposed to the linear block copolymer found in Pluronics. As depicted in Fig. S8 in the supplementary material, the curves with and without oil show minimal variation. Given that an oil shell does not present a significant source of error for fluorescence readings with 4-MU, it could be tested with the fucosylation inhibition assay on a DMF device.

One of the primary benefits of digital microfluidics is its potential for automation and standardization. Working toward this

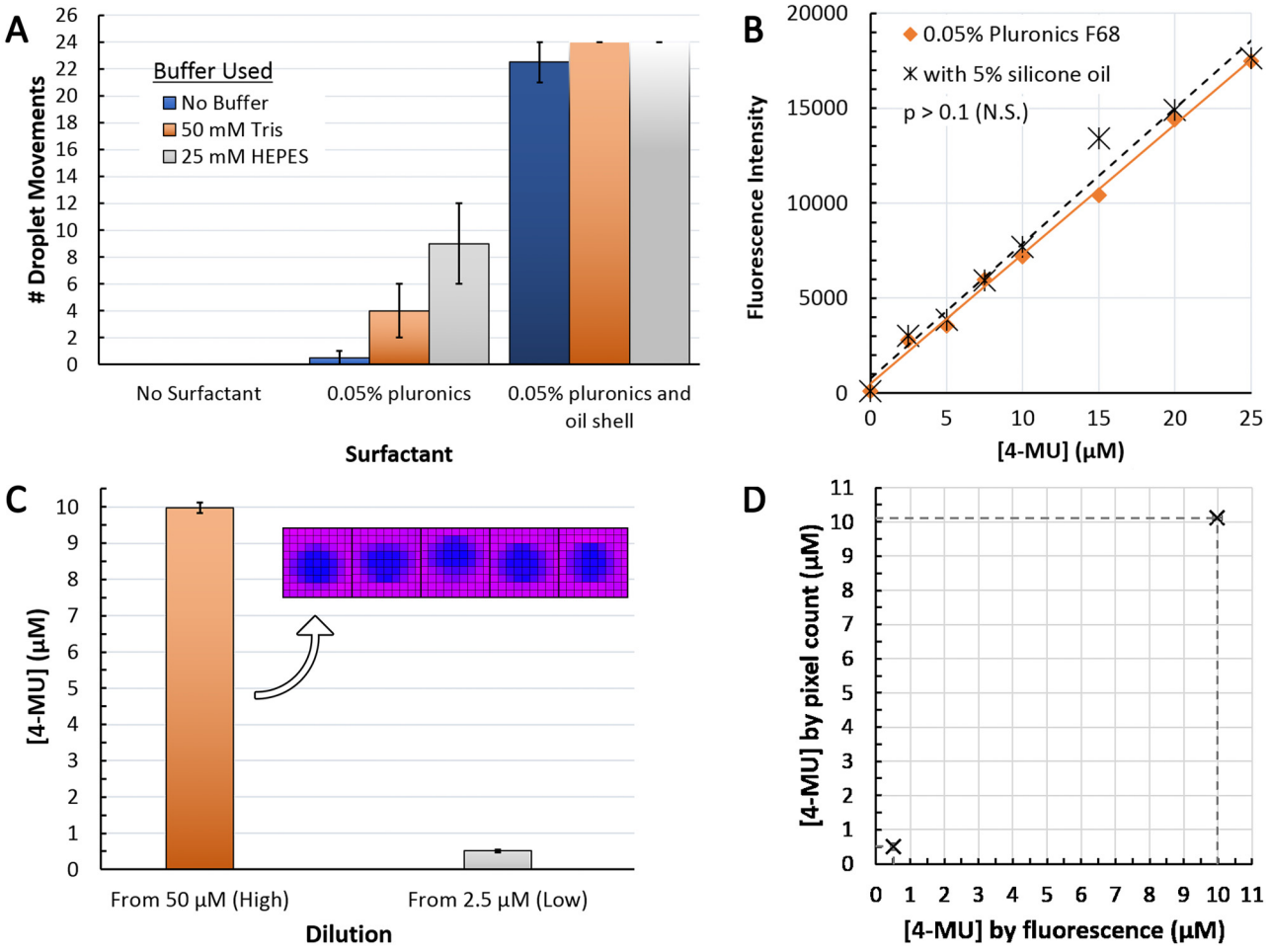

FIG. 3. Optimization of an inhibition assay. (a) Testing the effect of surfactant and oil on the movement of bulky protein solution (0.05 mg/ml BgaA). Each movement count represents the volume crossing an electrode over a span of four electrodes (n = 3). (b) The effect of oil on 4-MU standards with 0.05% F-68 Pluronics (n = 3). (c) A bar graph comparing the fluorescence of droplets diluted from two 4-MU concentrations (2.5 and 50 μM) to determine the homogeneity of the fluorescence for two concentrations of 4-MU (0.5 and 10 μM). Inset: Five images of droplets were taken using the well-plate reader showing the homogeneity of the droplets (n = 5). (d) Concentration of diluted 4-MU droplets calculated by fluorescence vs our pixel count method. 4-MU droplets calculated by fluorescence were done through 4-MU standards on-device. 4-MU droplets calculated by pixel count were done by dividing the initial calculated [4-MU] (by fluorescence) by the dilution factor calculated by pixel count (n = 5). All graphs with error bars represent one standard deviation.

initiative, we wanted to create a standard automated analysis tool with which we could directly calculate the concentrations in our samples instead of using inline detectors or external plate readers.[11,12] We created an image analysis method, referred to here as "pixel count" (PC), which visually measures the volumes on the device so that one may simply calculate the final concentration of the sample with $C_1V_1 = C_2V_2$. This standardized workflow consists of recording images of the device with any camera and using an edge-finding algorithm to determine droplet areas from which volume can be extrapolated (similar to the work by Vo *et al.*[15]). Using PC, initial volume (before dilution) and final volume (after dilution) could be determined. To validate PC, we first tested it against the volumes given by a micropipette and by a precision balance. A range of volumes (0.5–2 μl) were pipetted onto the device mounted on a precision balance, for which a change of weight reported the volume. The same range of volumes was pipetted onto a device that was covered by an ITO and then measured by PC. As shown in Fig. S9 in the supplementary material, the volumes calculated by PC are a closer match to those given by the micropipette and exhibited more precision than those reported by the precision balance. The next step was to ensure that droplets are being mixed homogenously and that the calculated concentration from PC matches with the concentration in the droplet. Hence, we tested by dispensing a ~500 nl droplet of 4-MU at high (50 μM) and

low (2.5 μM) concentrations into a 2.7 μl buffer. These volumes were then mixed on the device from each of the five droplets that were dispensed. As depicted in Fig. 3(c), the measured fluorescence of these diluted droplets shows a high degree of homogeneity. Fluorescence scans of the chip show minimal variability in the average fluorescence of the droplets dispensed from the same initial mixed droplet, <3% [Fig. 3(c) inset]. Finally, we compared our pixel count method to the gold standard of measuring fluorescence using a well-plate reader. As shown in Fig. 3(d), both low and high concentrations have excellent agreement in the 4-MU values when measured using both methods (<0.05% deviation). These values were calculated using a standard linear regression from 4-MU standards pipetted and measured on-device (Fig. S10 in the supplementary material). Using the PC method, we extrapolated the concentrations of solutions that were diluted on-device, which can potentially become a purely automated image-feedback-based process to keep track of any solute concentration at all steps of an experiment. Hence, the PC method created a standard workflow to analyze droplets on digital microfluidic devices, which can be done with any type of camera (without specialized detectors or a setup).

Testing of fucosylation assays on digital microfluidic devices

The development of tools to screen for inhibitors of fucosyltransferases could facilitate drug discovery, yielding treatments to combat metastasis, drug resistance and proliferation in cancers, host colonization by pathogens, chronic inflammation, and even autoimmune diseases such as asthma.[10,39] To evaluate the potential for testing inhibitors for fucosylation assays on digital microfluidic devices, we created a microfluidic system that generates a serial dilutions of the inhibitor, spanning at least four orders of magnitude. After optimizing conditions for this assay to be held on a digital microfluidic device, GDP was tested as a proof-of-concept inhibitor for FucT. Figure 4 shows the evaluation of the dose-responsive inhibitory activity of GDP, reported by fluorescence, together with well-plate results for comparison.

On the DMF device, droplets of six GDP concentrations were generated via serial ~5.5-fold dilutions along with 0 mM GDP as a blank. GDP concentrations were calculated using our developed PC method and 4-MU concentrations were calculated using our linear calibration curve (Fig. S10 in the supplementary material). After generation, each GDP droplet was mixed with a droplet containing FucT with a concentration of 0.03 mg/ml. Figure 4(a) shows the dose-response curve generated on the device for the GDP inhibition of FucT. The IC_{50} value obtained was 0.089 mM ± 0.092. Similarly, we implemented the same assay in a well plate and achieved an IC_{50} value of 0.015 mM ± 0.029 [Fig. 4(b)]. It was observed that at the highest concentration of GDP (40 mM) on both platforms, fluorescence intensity had dropped by nearly half relative to the next highest concentration (a 20 mM GDP reaction). Removing the ~40 mM GDP reactions from the dataset returned IC_{50} values closer to expectation without the decline in the curve (IC_{50} = 0.108 mM ± 0.205 in the well plate and IC_{50} = 0.180 mM ± 0.199 on the DMF device). Typically, this reversal of response to inhibitor concentration is attributed to bell-shaped dose–response curves, in which multiple binding sites, multiple targets, or the aggregation of drug into

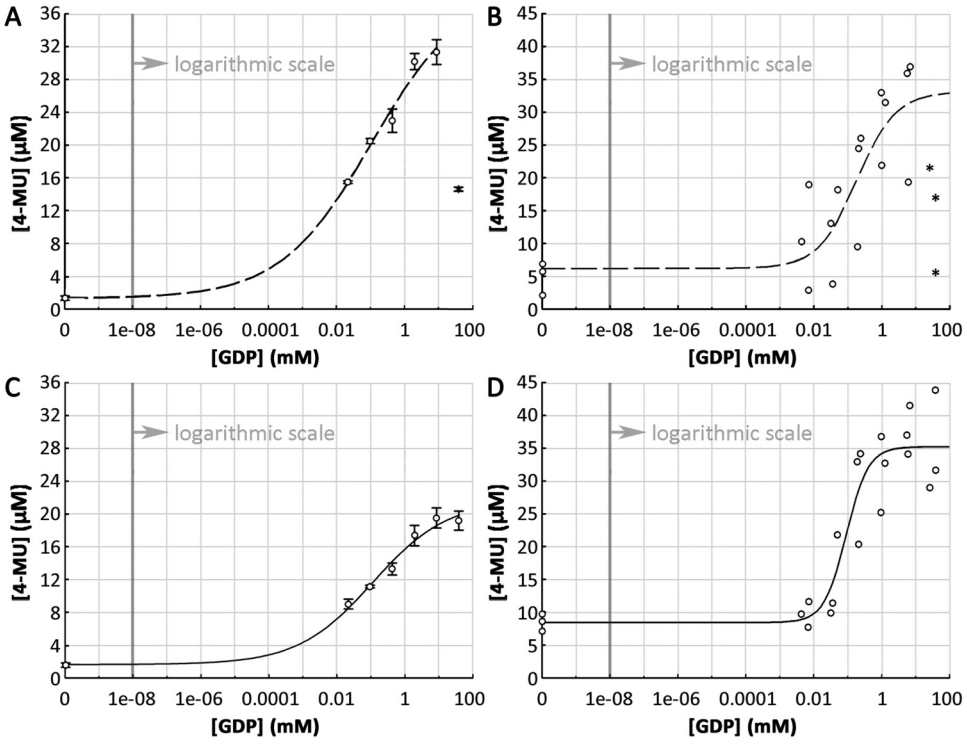

FIG. 4. Testing: inhibition curves of FucT by GDP. Well-plate and DMF assays both performed at 0.05% Pluronics with droplets coated with silicone oil shell. Sigmoid curves and corresponding IC_{50} were drawn and fitted to the formula $y = b + ((a - b)/(1 + (x/c)^d))$ using a least squares routine. IC_{50} curves in a well plate, before (a) and after (c) glycine dilution (n = 3). IC_{50} curves on a DMF device, before (b) and after (d) glycine dilution (n = 3). All graphs with error bars represent one standard deviation. Star marks [(a) and (b)] represent 40 mM GDP inhibitor concentrations that were excluded as outliers in the IC_{50} calculation.

colloids at certain concentrations negatively impacts inhibition after inhibitor concentration crosses above a certain threshold (i.e., peak inhibition).[40] Given that 4-MU is prone to shifts in its emissions peak in response to differences in ionic conditions, pH, and % water content, it was also hypothesized that the bell-shaped dose–response curve was not due to differences in inhibition, but rather due to the quenching effect of concentrated GDP upon 4-MU. To test our speculation, we equilibrated assay solutions by subjecting them to a 5-fold dilution in pH 10.4 1M glycine. As shown in Figs. 4(c) and 4(d), this immediately restored the curve to a sigmoidal fit when performed, both on the well plate and on the DMF device. The values reported by the inhibition assay after glycine dilution were relatively consistent with each other at 0.114 mM ± 0.086 on well plates and 0.093 mM ± 0.037 on DMF devices (N.S.: $p = 0.53$, $\alpha = 0.05$). We believe that with glycine dilution, the viscosity of the solutions changes, which gives rise to better reproducibility in dispensing droplets and more consistent measurements (i.e., smaller errors).

Even prior to glycine dilution, reaction solutions in both the well plate and the DMF altered 4-MU fluorescence intensity. This was higher than the theoretical maximum given by the concentration of fluorogenic MU-β-LacNAc present in the solution (diluted from its 10 μM reaction concentration to 7.5 μM at the end of the assay). Since the 4-MU standards had been prepared with the same buffer and surfactant conditions as those of the samples, it suggests that the reaction components (i.e., buffer and surfactant) might enhance 4-MU fluorescence. We note that 4-MU fluorescence is sensitive to differences in solvent and ionic conditions. Regardless, these DMF methods could be used to automate the collection of IC_{50} data with inhibition curves spanning several orders of magnitude (and with smaller volumes[9]), which is conducive for plans to implement the automated screening for potential inhibitors of fucosyltransferases.

CONCLUSION

We report here the first application of digital microfluidics and image-based analysis to report the inhibition of fucosylation. In this work, we conducted proof-of-concept testing for a novel fucosylation inhibition assay using the fluorogenically labeled synthetic disaccharide, MU-β-LacNAc. This disaccharide was shown to be a useful probe for fucosylation by *H. pylori* FucT, with potential for high-throughput application. GDP was used as a test inhibitor and subjected to serial dilution spanning four orders of magnitude on the DMF device. The image-based tool produced dose–response curves with associated IC_{50} values that were comparable to results on well plates. We also showed results related to optimizing the device conditions for performing the assay, such as electrode design, testing the effects of surfactants and oil on droplet movement, and dispensing variability of the reagents. We also validated our standardized image-based analysis tool (called "pixel count") with which we directly calculated the constituent concentrations of the droplets on-device. Finally, we conclude that there is great potential for the development of an automated and standardized enzyme inhibition assay platform, and this work represents an important first step toward future screens for inhibitors of multiple types of fucosyltransferases.

SUPPLEMENTARY MATERIAL

The supplementary material contains protocols for transformation, protein expression, and purification of *Abg2F6, BgaA, SpHex, and FucT* expression strains, enzymatic synthesis and purification of *MU-β-LacNAc*, DMF device fabrication, and the construction of electrode sequences using PaseMaker (a software for automating droplet movement). The supplementary material also contains figures and tables showing how to construct the automation hardware, implementation of the software for droplet movement on device, steps on how to perform the fucosylation assay on-chip, errors in droplet dispensing on device, inhibition curve of FucT by GDP, electrode shape designs tested in this study, the effect of Tetronics surfactant with and without oil on 4-MU fluorescence, accuracy and precision of pixel count method, and a calibration curve to correlate 4-MU concentration with fluorescence.

ACKNOWLEDGEMENTS

We thank the Natural Sciences and Engineering Research Council (NSERC) (No. RGPIN-2016-06712 to S.C.C.S. and No. RGPIN-2016-05464 to D.H.K.), the Fonds de Recherche Nature et technologies (FRQNT) (No. 204862 to S.C.C.S. and No. 197819 to D.H.K.), the Canadian Glycomics Network (NCE-2016-280035 to D.H.K.), and the Canadian Foundation of Innovation (CFI) (No. 35649) for funding. We thank Concordia University's Biology Department and the Department of Electrical and Computer Engineering for their funding and academic resources.

REFERENCES

[1]K. S. Lau, E. A. Partridge, A. Grigorian, C. I. Silvescu, V. N. Reinhold, M. Demetriou, and J. W. Dennis, Cell **129**(1), 123–134 (2007).
[2]Z. Tu, Y. N. Lin, and C. H. Lin, Chem. Soc. Rev. **42**(10), 4459–4475 (2013).
[3]X. Feng, L. Zhao, S. Gao, X. Song, W. Dong, Y. Zhao, H. Zhou, L. Cheng, X. Miao, and L. Jia, Gene **578**(2), 232–241 (2016).
[4]N. Very, T. Lefebvre, and I. El Yazidi-Belkoura, Oncotarget **9**(1), 1380–1402 (2018).
[5]D. P. McGovern, M. R. Jones, K. D. Taylor, K. Marciante, X. Yan, M. Dubinsky, A. Ippoliti, E. Vasiliauskas, D. Berel, C. Derkowski, D. Dutridge, P. Fleshner, D. Q. Shih, G. Melmed, E. Mengesha, L. King, S. Pressman, T. Haritunians, X. Guo, S. R. Targan, J. I. Rotter, and International IBD Genetics Consortium, Hum. Mol. Genet. **19** (17), 3468–3476 (2010).
[6]J. Zhang, N. Ju, X. Yang, L. Chen, and C. Yu, Life Sci. **192**, 231–237 (2018).
[7]R. Norden, E. Samuelsson, and K. Nystrom, Glycobiology **27**(11), 999–1005 (2017).
[8]M. Boziki, S. A. Polyzos, G. Deretzi, E. Kazakos, P. Katsinelos, M. Doulberis, G. Kotronis, E. Giartza-Taxidou, L. Laskaridis, D. Tzivras, E. Vardaka, C. Kountouras, N. Grigoriadis, R. Thomann, and J. Kountouras, Neurochem. Int. **113**, 137–151 (2018).
[9]C. D. Rillahan, S. J. Brown, A. C. Register, H. Rosen, and J. C. Paulson, Angew. Chem. Int. Ed. Engl. **50**(52), 12534–12537 (2011).
[10]X. Zhang, F. Chen, A. Petrella, F. Chacon Huete, J. Covone, T. W. Tsai, C. C. Yu, P. Forgione, and D. H. Kwan, ACS Chem. Biol. **14**(4), 715–724 (2019).
[11]M. Husser, P. Q. N. Vo, H. Sinha, F. Ahmadi, and S. C. C. Shih, ACS Synth. Biol. **7**, 933–944 (2018).
[12]F. Ahmadi, K. Samlali, P. Q. N. Vo, and S. C. C. Shih, Lab Chip **19**(3), 524–535 (2019).
[13]S. Nayak, N. R. Blumenfeld, T. Laksanasopin, and S. K. Sia, Anal. Chem. **89**(1), 102–123 (2017).

[14]R. Fobel, C. Fobel, and A. R. Wheeler, Appl. Phys. Lett. **102**(19), 193513 (2013).
[15]P. Q. N. Vo, M. C. Husser, F. Ahmadi, H. Sinha, and S. C. C. Shih, Lab Chip **17**(20), 3437–3446 (2017).
[16]Y. Liu and I. Papautsky, Micromachines **10**(2), 107 (2019).
[17]C. Graham, R. S. Sista, J. Kleinert, N. Wu, A. Eckhardt, D. Bali, D. S. Millington, and V. K. Pamula, Clin. Biochem. **46**(18), 1889–1891 (2013).
[18]S. Kalsi, M. Valiadi, C. Turner, M. Sutton, and H. Morgan, Lab Chip **19**(1), 168–177 (2018).
[19]S. L. Freire and B. Tanner, Langmuir **29**(28), 9024–9030 (2013).
[20]M. K. Sarvothaman, K. S. Kim, B. Seale, P. M. Brodersen, G. C. Walker, and A. R. Wheeler, Adv. Funct. Mater. **25**(4), 506–515 (2015).
[21]H. Yu, Y. Li, Z. Wu, L. Li, J. Zeng, C. Zhao, Y. Wu, N. Tasnima, J. Wang, H. Liu, M. R. Gadi, W. Guan, P. G. Wang, and X. Chen, Chem. Commun. **53**(80), 11012–11015 (2017).
[22]H. Sinha, A. B. V. Quach, P. Q. N. Vo, and S. C. C. Shih, Lab Chip **18**(15), 2300–2312 (2018).
[23]D. G. Rackus, R. P. S. de Campos, C. Chan, M. M. Karcz, B. Seale, T. Narahari, C. Dixon, M. D. Chamberlain, and A. R. Wheeler, Lab Chip **17**(13), 2272–2280 (2017).
[24]A. K. Singh, B. Pluvinage, M. A. Higgins, A. B. Dalia, S. A. Woodiga, M. Flynn, A. R. Lloyd, J. N. Weiser, K. A. Stubbs, A. B. Boraston, and S. J. King, PLoS Pathog. **10**(9), e1004364 (2014).
[25]B. L. Mark, G. A. Wasney, T. J. Salo, A. R. Khan, Z. Cao, P. W. Robbins, M. N. James, and B. L. Triggs-Raine, J. Biol. Chem. **273**(31), 19618–19624 (1998).
[26]T. de Vries, R. M. Knegtel, E. H. Holmes, and B. A. Macher, Glycobiology **11**(10), 119R–128R (2001).
[27]C. H. Wong, D. P. Dumas, Y. Ichikawa, K. Koseki, S. J. Danishefsky, B. W. Weston, and J. B. Lowe, J. Am. Chem. Soc. **114**(18), 7321–7322 (1992).
[28]F. Zou, Q. Ruan, X. Lin, M. Zhang, Y. Song, L. Zhou, Z. Zhu, S. Lin, W. Wang, and C. J. Yang, Biosens. Bioelectron. **126**, 551–557 (2019).
[29]D. Brassard, L. Malic, F. Normandin, M. Tabrizian, and T. Veres, Lab Chip **8**(8), 1342–1349 (2008).
[30]N. Vergauwe, D. Witters, Y. T. Atalay, B. Verbruggen, S. Vermeir, F. Ceyssens, R. Puers, and J. Lammertyn, Microfluid. Nanofluid. **11**(1), 25–34 (2011).
[31]E. Moazami, J. M. Perry, G. Soffer, M. C. Husser, and S. C. C. Shih, Anal. Chem. **91**(8), 5159–5168 (2019).
[32]S. H. Au, P. Kumar, and A. R. Wheeler, Langmuir **27**(13), 8586–8594 (2011).
[33]V. N. Luk, G. Mo, and A. R. Wheeler, Langmuir **24**(12), 6382–6389 (2008).
[34]J. Y. Yoon and R. L. Garrell, Anal. Chem. **75**(19), 5097–5102 (2003).
[35]M. F. Samad, A. Z. Kouzani, M. F. Hossain, M. I. Mohammad, and M. N. H. Alam, Microsyst. Technol. **23**(7), 3005–3013 (2017).
[36]J. Berthier and C. Peponnet, Biomicrofluidics **1**(1), 014104 (2007).
[37]M. Abdelgawad, P. Park, and A. R. Wheeler, J. Appl. Phys. **105**, 094506 (2009).
[38]N. Rajabi and A. Dolatabadi, Colloid Surf. A **365**, 230–236 (2010).
[39]Z. Gao, O. G. Ovchinnikova, B. S. Huang, F. Liu, D. E. Williams, R. J. Andersen, T. L. Lowary, C. Whitfield, and S. G. Withers, J. Am. Chem. Soc. **141**(6), 2201–2204 (2019).
[40]S. C. Owen, A. K. Doak, A. N. Ganesh, L. Nedyalkova, C. K. McLaughlin, B. K. Shoichet, and M. S. Shoichet, ACS Chem. Biol. **9**(3), 777–784 (2014).